

# Fast Local LUT Upsampling

Hiroshi Tajima, Teppei Tsubokawa, Yoshihiro Maeda, and Norishige Fukushima \*

*Nagoya Institute of Technology, Japan, Tokyo University of Science, Japan*

\* <https://fukushima.web.nitech.ac.jp/en/>

Keywords: Edge-preserving filtering, local LUT upsampling, acceleration, bilateral filtering,  $L_0$  smoothing

Abstract: Edge-preserving filters have been used in various applications in image processing. As the number of pixels of digital cameras has been increasing, the computational cost becomes higher, since the order of the filters depends on the image size. There are several acceleration approaches for the edge-preserving filtering; however, most approaches reduce the dependency of filtering kernel size to the processing time. In this paper, we propose a method to accelerate the edge-preserving filters for high-resolution images. The method subsamples an input image and then performs the edge-preserving filtering on the subsampled image. Our method then upsamples the subsampled image with the guidance, which is the high-resolution input images. For this upsampling, we generate per-pixel LUTs for high-precision upsampling. Experimental results show that the proposed method has higher performance than the conventional approaches.

## 1 INTRODUCTION

Edge-preserving filtering smooths images while maintaining the outline in the images. There are various edge-preserving filters for various purposes of image processing, such as bilateral filtering (Tomasi and Manduchi, 1998), non-local means filtering (Buades et al., 2005), DCT filtering (Yu and Sapiro, 2011), BM3D (Dabov et al., 2007), guided image filtering (He et al., 2010), domain transform filtering (Gastal and Oliveira, 2011), adaptive manifold filtering (Gastal and Oliveira, 2012), local Laplacian filtering (Paris et al., 2011), weighted least square filtering (Levin et al., 2004), and  $L_0$  smoothing (Xu et al., 2011). The applications of the edge-preserving filters include noise removal (Buades et al., 2005), outline emphasis (Bae et al., 2006), high dynamic range imaging (Durand and Dorsey, 2002), haze removing (He et al., 2009), stereo matching (Hosni et al., 2013; Matsuo et al., 2015), free viewpoint imaging (Kodera et al., 2013), depth map enhancement (Matsuo et al., 2013).

The computational cost is the main issue in the research of edge-preserving filtering. There are several acceleration approaches for each filter, such as bilateral filtering (Durand and Dorsey, 2002; Yang et al., 2009; Adams et al., 2010; Chaudhury et al., 2011; Chaudhury, 2011; Chaudhury, 2013; Sugimoto and Kamata, 2015; Sugimoto et al., 2016; Ghosh et al., 2018; Maeda et al., 2018b; Maeda et al., 2018a; Sugi-

moto et al., 2019; Fukushima et al., 2019b), non-local means filtering (Adams et al., 2010; Fukushima et al., 2015), local Laplacian filtering (Aubry et al., 2014), DCT filtering (Fujita et al., 2015; Fukushima et al., 2019a), guided image filtering (Murooka et al., 2018; Fukushima et al., 2018) and weighted least square filtering (Min et al., 2014). The computational time of each filter, however, depends on image resolution, and it is rapidly increasing, e.g., a camera in cellphone even have 12M pixels. For such a high-resolution image, we require more acceleration techniques.

Processing with subsampling and then upsampling is the most straightforward approach to accelerate image processing. This approach dramatically reduces processing time; however, the accuracy of the approximation is also significantly decreased. Subsampling loses high-frequency and large edges in images; hence, the resulting images also lose the information. Different from super-resolution problems, subsampling/upsampling for acceleration can utilize a high-resolution input image as a guidance signal. Joint bilateral upsampling (Kopf et al., 2007) and guided image upsampling (He and Sun, 2015) utilize the high-resolution image for high-quality upsampling as extensions of joint bilateral filtering (Petschnigg et al., 2004; Eisemann and Durand, 2004). However, both upsampling methods are specific for accelerating bilateral filtering and guided image filtering. More application-specific upsampling, e.g., depth map upsampling (Fukushima et al., 2016),

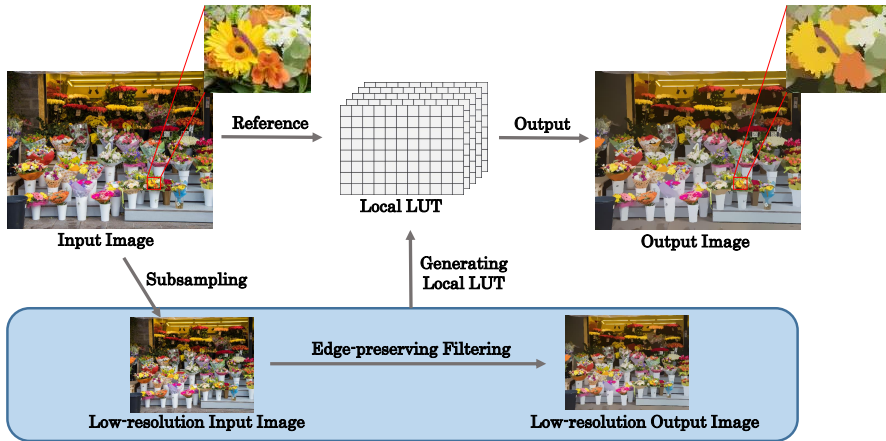


Figure 1: Local LUT upsampling: an input image is downsampled, and then the image is smoothed by arbitrary edge-preserving filtering. Next, we create per-pixel LUTs by using the correspondence between subsampled input and output images. Finally, we convert the input image into the approximated image by the LUT.

improves the upsampling quality.

To accelerate arbitrary edge-preserving filtering, we proposed a new upsampling method named fast local look-up table (LUT) upsampling, which has higher accuracy with fast computational ability than the conventional method (Tajima et al., 2019). Figure 1 indicates an overview of our method. In the method, edge-preserving filtering, which has the highest cost in the processing, is performed in the downsampled domain for acceleration. Then our method utilizes high-resolution information for accurate upsampling.

This work is an extension of our previous work (Tajima et al., 2019). The contribution of this work is improving the computational method of per-pixel LUT to achieve better accuracy with saving computational time than conventional work. Also, the proposed method is justified by state-of-the-arts upsampling methods (Chen et al., 2016).

## 2 LOCAL LUT

### 2.1 Concept of Local LUT

We review the concept of local LUT upsampling. Usually, image intensity transformation by using LUT, such as contrast enhancement, gamma correction, and tone mapping, we use a LUT for each pixel. We call this method as global LUT. The global LUT can represent any point-wise operations for each pixel, but this approach cannot represent area-based operations, such as image filtering.

By contrast, our approach of the local LUT generates per-pixel LUTs. The LUT maps pixel values of

the input image to that of an image processing result. The local LUT  $T$  at a pixel  $p$  has following relationship between an input image  $I$  and an output image  $J$ .

$$J_p = T_p[I_p], \quad (1)$$

where  $T[\cdot]$  represents LUT reference operation. If we have the output of edge-preserving filtering, we can easily transform the input image into the edge-preserving result by referring the LUT. It is nonsense that the output image is required for generating the output image itself. Therefore, we generate the local LUT in the subsampled image domain for acceleration. The proposed method generates per-pixel LUTs for the function from the correspondence between a subsampled input image and its filtering result.

The local LUT for each pixel is created from neighboring pairs of low-resolution input and output image around a target pixel. Luminance values around the neighboring region have high correlations. Also, the correlation between the output of filtering and the input image becomes high. Therefore we aggregate the mapping relationship around neighboring pixels.

Figure 2 shows the scatter plot of intensity pair between a local patch of an input image and a filtered image. The correspondence map almost represents the local LUT, but there are two issues; multiple output candidates and gap issues. LUT requires one-to-one mapping for each intensity of input and output, but this scatter plot represents one-to-zero or one-to- $n$  matching. Our previous work (Tajima et al., 2019) and this work solves the issues.

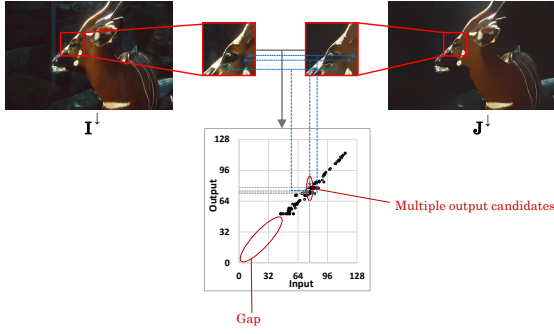


Figure 2: Issues in generating local LUT: We make a scatter-plot for correspondence between input and output subsampled images in a local window. The scatter-plot almost represents the LUT for mapping input to output. But there are two problems; gap and multiple-output candidates.

## 2.2 Conventional Approach

We shortly introduce the computing method of the local LUT in (Tajima et al., 2019). Initially, an input image  $I$  is subsampled to generate a low-resolution input image  $I_\downarrow$ :

$$I_\downarrow = S_s(I), \quad (2)$$

where  $S_s$  is a subsampling operator. Then, edge-preserving filtering is applied for  $I_\downarrow$  and the subsampled output  $J_\downarrow$  is obtained as follows:

$$J_\downarrow = F(I_\downarrow), \quad (3)$$

where  $F$  is an operator of arbitrary edge-preserving filtering. Then, we create a local LUT on a pixel from the correspondence between  $I_\downarrow$  and  $J_\downarrow$ . Let be  $p_\downarrow$  the target pixel in the subsampled images of  $I_\downarrow$  and  $J_\downarrow$ . The local LUT on  $p_\downarrow$  is defined as follows:

$$\mathbf{T}_{p_\downarrow} = \text{Func}\{I_\downarrow, J_\downarrow, p_\downarrow, W_{p_\downarrow}\}, \quad (4)$$

where  $W_{p_\downarrow}$  is a set of neighboring pixels around  $p_\downarrow$ .  $\text{Func}\{\cdot\}$  indicates each approach for generating the local LUT.

Here, we review two conventional approaches to generating the local LUT, which is proposed in (Tajima et al., 2019). The first one is the dynamic programming approach (DP). This approach simultaneously solves the problems of gap and multiple-candidates. This algorithm is shown in Algorithm 1. In the approach, we count frequency of one-to-one mapping of intensity between the images  $I_\downarrow$  and  $J_\downarrow$  in local window  $W_{p_\downarrow}$ . Let introduce a frequency map  $f_{p_\downarrow}(s, t)$  on a pixel  $p_\downarrow$ , where  $s$  and  $t$  are an intensity value on  $I_\downarrow$  and  $J_\downarrow$ , respectively. The frequency is counted by gathering around a pixel  $W_{p_\downarrow}$ .

Also, we consider quantization of the intensity for acceleration.  $S_c(x)$  is a quantization function and defined by:

$$S_c(x) = \lfloor x/l \rfloor \quad (5)$$

---

### Algorithm 1 : DP approach

---

**Input:**  $I_\downarrow, J_\downarrow, p_\downarrow, W_{p_\downarrow}$

**Initialization:**  $N = (2r + 1)^2$

**Initialization:**  $L =$  the number of bins

**Initialization:**  $f_{p_\downarrow}(s, t) = 0 \forall s, t$

Let  $q_\downarrow$  be a neighboring pixel ( $\{q_{1\downarrow}, \dots, q_{N\downarrow}\} \in W_{p_\downarrow}$ )

**For** ( $n = 1$  to  $N$ )

$f_{p_\downarrow}(S_c(I_{q_{n\downarrow}}), S_c(J_{q_{n\downarrow}})) ++$

**For** ( $i = 1$  to  $L - 1$ )

$f_{p_\downarrow}(i, 0) += f_{p_\downarrow}(i - 1, 0)$

$f_{p_\downarrow}(0, i) += f_{p_\downarrow}(0, i - 1)$

**For** ( $s = 1$  to  $L - 1$ )

**For** ( $t = 1$  to  $L - 1$ )

$C_1 = f_{p_\downarrow}(s - 1, t - 1) + O$

$C_2 = f_{p_\downarrow}(s - 1, t)$

$C_3 = f_{p_\downarrow}(s, t - 1)$

$f_{p_\downarrow}(s, t) = \max(C_1, C_2, C_3) + f_{p_\downarrow}(s, t)$

$index(s, t) = \arg \max_m C_m (m = 1, 2, 3)$

$s = L - 1, t = L - 1$

**While** ( $s \geq 0$  and  $t \geq 0$ )

$\mathbf{T}_{p_\downarrow}[s] = t$

**Switch**( $index(s, t)$ )

1 :  $s --, t --$

2 :  $s --$

3 :  $t --$

---



---

### Algorithm 2 : WTA approach

---

**Input:**  $I_\downarrow, J_\downarrow, p_\downarrow, W_{p_\downarrow}$

**Initialization:**  $N = (2r + 1)^2$

**Initialization:**  $L =$  the number of bins

**Initialization:**  $f_{p_\downarrow}(s, t) = 0 \forall s, t$

Let  $q_\downarrow$  be a neighboring pixel ( $\{q_{1\downarrow}, \dots, q_{N\downarrow}\} \in W_{p_\downarrow}$ )

**For** ( $n = 1$  to  $N$ )

$f_{p_\downarrow}(S_c(I_{q_{n\downarrow}}), S_c(J_{q_{n\downarrow}})) ++$

**For** ( $s = 0$  to  $L - 1$ )

$\mathbf{T}_{p_\downarrow}[s] = \arg \max_t f_{p_\downarrow}(s, t)$

**For** ( $s = 0$  to  $L - 1$ )

**If** ( $\mathbf{T}_{p_\downarrow}[s] = 0$ )

$Interpolate(\mathbf{T}_{p_\downarrow}[s])$

---

where  $l$  is a quantization parameter. The output of the local LUT has  $256/l$  dimensions. We call the number of intensity candidates as the number of bins.

After constructing the frequency map, we optimize the result by using DP. The parameter  $O$  in Algorithm 1 represents an offset value to enforce diagonal matching. The cost function of  $f$  can be recursively updated. After filling the cost function, we trace back the function to determine a solid pass. Note that DP approach ensures the monotonicity in the local LUT.

The second approach is the winner-takes-all ap-

proach (WTA). The algorithm is shown in Algorithm 2. In this approach, the output value of  $\mathbf{T}_{\mathbf{p}_\downarrow}[s]$  is determined as the most frequent intensity in the output image for intensity  $s$  in the input image. However, this approach still has the gap problem in the LUT; thus, we interpolate the gap. ”*Interpolate*( $\cdot$ )” in the algorithm indicates linearly interpolating between the nearest existing values in bins. For the boundary condition of interpolation, we set  $\mathbf{T}_{\mathbf{p}_\downarrow}[0] = 0$  and  $\mathbf{T}_{\mathbf{p}_\downarrow}[255] = 255$ . The solution cannot keep monotonicity for the local LUT. The fact sometimes generates negative edges.

After WTA and DP, the matrix indicates one-to-one mapping. We call this per-pixel mapping function  $\mathbf{T}_{\mathbf{p}_\downarrow}$  as local LUT. These approaches require a frequency map, i.e., 2D histogram. The number of elements in the map is  $L^2$ . Usually,  $L = 256$  for no-range downsampling case, we initialize 65536 elements per each pixel by setting 0. By contrast, the size of the local window is  $r \times r$ , and typically  $r = 2, 3, 4$ , or 5. Thus, the size of the frequency map is dominant. Also, the cost of memory access for more massive array has higher than arithmetic operations in current computers (Hennessy and Patterson, 2017).

### 3 PROPOSED METHOD

#### 3.1 Fast Local LUT

In this section, we propose an acceleration method of local LUT computation. For acceleration, we remove the computing process of the frequency map counting from the algorithm. We call the new approach fast local LUT (FLL).

In FLL, we solve the multiple-candidates problem in the local LUT computation by giving priority to the correspondence matching. The priority is the nearness of distance between a target pixel position and reference pixel position of neighborhood pixels. If we have multiple candidates, we adopt the intensity of the pixel where locates the nearest position from the center of the local window. With this priority, we can directly compute a local LUT on a pixel without counting the frequency map.

We implemented two methods to solve the local LUT with the nearness priority. Note that both two methods have the same result. The first implementation is raster scan order computation. This approach determines the output values of the local LUT by scanning the local window with the raster scan order. The algorithm 3 shows this method. In this method, we compare spatial distance of  $L_1$  norm between  $\mathbf{p}_\downarrow$  and  $\mathbf{q}_{n\downarrow}$ , when  $\mathbf{T}_{\mathbf{p}_\downarrow}[S_c(\mathbf{I}_{\mathbf{q}_{n\downarrow}})]$  already has the output

---

#### Algorithm 3 : FLL (Raster scan)

---

**Input:**  $\mathbf{I}_\downarrow, \mathbf{J}_\downarrow, \mathbf{p}_\downarrow, W_{\mathbf{p}_\downarrow}$   
**Initialization:**  $N = (2r + 1)^2$   
**Initialization:**  $L =$  the number of bins  
Let  $\mathbf{q}_\downarrow$  be a neighboring pixel ( $\{\mathbf{q}_{1\downarrow}, \dots, \mathbf{q}_{N\downarrow}\} \in W_{\mathbf{p}_\downarrow}$ )  
**For** ( $n = 1$  **to**  $N$ )  
     $distance[n] = |\mathbf{p}_\downarrow - \mathbf{q}_{n\downarrow}|$  //computable in advance  
**For** ( $n = 1$  **to**  $N$ )  
    **If** ( $\mathbf{T}_{\mathbf{p}_\downarrow}[S_c(\mathbf{I}_{\mathbf{q}_{n\downarrow}})] = \text{NULL}$ )  
         $\mathbf{T}_{\mathbf{p}_\downarrow}[S_c(\mathbf{I}_{\mathbf{q}_{n\downarrow}})] = S_c(\mathbf{J}_{\mathbf{q}_{n\downarrow}})$   
         $index[S_c(\mathbf{I}_{\mathbf{q}_{n\downarrow}})] = distance[n]$   
    **Else**  
        **If** ( $distance[n] \leq index[S_c(\mathbf{I}_{\mathbf{q}_{n\downarrow}})]$ )  
             $\mathbf{T}_{\mathbf{p}_\downarrow}[S_c(\mathbf{I}_{\mathbf{q}_{n\downarrow}})] = S_c(\mathbf{J}_{\mathbf{q}_{n\downarrow}})$   
             $index[S_c(\mathbf{I}_{\mathbf{q}_{n\downarrow}})] = distance[n]$   
**For** ( $s = 0$  **to**  $L - 1$ )  
    **If** ( $\mathbf{T}_{\mathbf{p}_\downarrow}[s] = 0$ )  
         $Interpolate(\mathbf{T}_{\mathbf{p}_\downarrow}[s])$

---



---

#### Algorithm 4 : FLL (Spiral)

---

**Input:**  $\mathbf{I}_\downarrow, \mathbf{J}_\downarrow, \mathbf{p}_\downarrow, W_{\mathbf{p}_\downarrow}$   
**Initialization:**  $k = 0, N = (2r + 1)^2$   
**Initialization:**  $L =$  the number of bins  
Let  $\mathbf{q}_\downarrow$  be a neighboring pixel ( $\{\mathbf{q}_{1\downarrow}, \dots, \mathbf{q}_{N\downarrow}\} \in W_{\mathbf{p}_\downarrow}$ )  
**For** ( $n = 1$  **to**  $N$ )  
     $distance[n] = |\mathbf{p}_\downarrow - \mathbf{q}_{n\downarrow}|$  //computable in advance  
**For** ( $d = 2r$  **to** 0)  
    **For** ( $n = 1$  **to**  $N$ )  
        **If** ( $distance[n] = d$ )  
             $s\_index[k++] = n$  //computable in advance  
**For** ( $i = 1$  **to**  $N$ )  
     $n = s\_index[i]$   
     $\mathbf{T}_{\mathbf{p}_\downarrow}[S_c(\mathbf{I}_{\mathbf{q}_{n\downarrow}})] = S_c(\mathbf{J}_{\mathbf{q}_{n\downarrow}})$   
**For** ( $s = 0$  **to**  $L - 1$ )  
    **If** ( $\mathbf{T}_{\mathbf{p}_\downarrow}[s] = 0$ )  
         $Interpolate(\mathbf{T}_{\mathbf{p}_\downarrow}[s])$

---

value. Therefore, this method has two comparing operations, i.e., NULL check and distance comparison.

The second implementation is that determines output values of local LUT in the spiral scanning order. Generating this order, we sort the pair of input and output intensity by the key of  $L_1$  norm distance between  $\mathbf{p}_\downarrow$  and  $\mathbf{q}_{n\downarrow}$  with descending order. Algorithm 4 shows the algorithm of this method. In this method, the value is overwritten by a new one, even if  $\mathbf{T}_{\mathbf{p}_\downarrow}[S_c(\mathbf{I}_{\mathbf{q}_{n\downarrow}})]$  already has the output value, because new one in the sorted order must have the nearer distance than the previous one. Therefore, there is no comparing operation. Besides, the sorted order is computable in advance and only computes at once; thus, this method additionally reduces computational

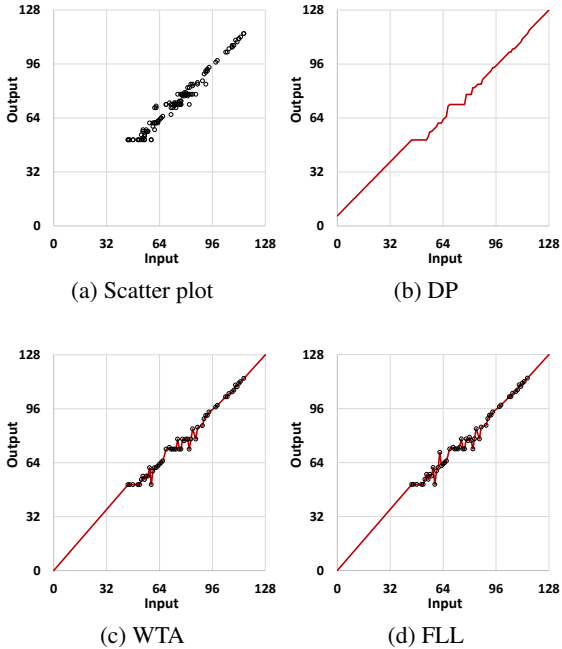


Figure 3: Scatter plot of input and output values and results of each approach for generating local LUT on  $\mathbf{p}$ . The number of bins is 128, i.e., quantization level is  $l = 2$ . The radius of neighboring pixels is  $r = 5$ . The subsampling rate is  $1/16$ .

time.

Figure 3 shows the generated local LUT of each approach, i.e., DP, WTA, and FLL.

### 3.2 Upsampling of Local LUT

The local LUT has three-dimensional information, such as  $n$ ,  $\mathbf{p} = (x, y)$ ; however, all elements are subsampled. It has not enough to map an input image into an output image in a high-resolution image. Therefore, we upsample the local LUT to intensity and spatial dimension. The upsampling is defined as follows:

$$\tilde{\mathbf{T}} = \mathcal{S}_c^{-1}(\mathcal{S}_s^{-1}(\mathbf{T}_\downarrow)), \quad (6)$$

where  $\tilde{\mathbf{T}}$  and  $\mathbf{T}_\downarrow$  are tensors, which gathers each local LUT for each pixels.  $\mathcal{S}_c^{-1}(\cdot)$  and  $\mathcal{S}_s^{-1}(\cdot)$  are tensor upsampling operators for the intensity and spatial domain of the tensors, respectively. Finally, the output image is generated by referring to the local LUT and input intensity of  $\mathbf{I}_p$ . The output is defined by:

$$\mathbf{J}_p = \tilde{\mathbf{T}}_p[\mathbf{I}_p]. \quad (7)$$

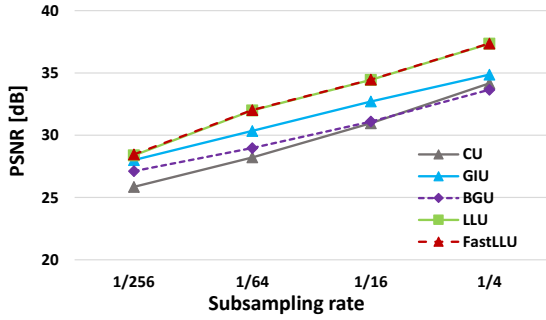
For intensity and spatial domain upsampling, we used linear upsampling for intensity, and bilinear or bicubic upsampling for spatial domain. We call linear-bilinear pair as tri-linear upsampling, and linear-bicubic pair as linear-bicubic upsampling.

## 4 EXPERIMENTAL RESULTS

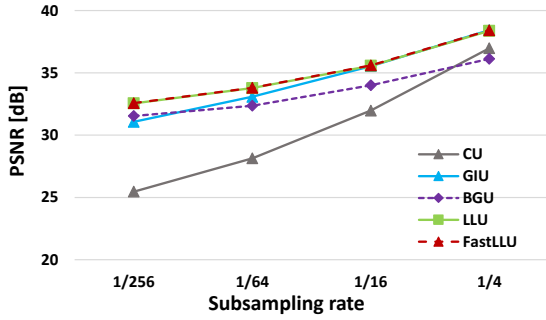
We accelerated two edge-preserving filters, such as iterative bilateral filtering and  $L_0$  smoothing by subsampling based acceleration methods. These filters can mostly smooth images; however, the computational cost is high. We compared the proposed method of the local LUT upsampling with the conventional method of the cubic upsampling (CU), guided image upsampling (GIU) (He and Sun, 2015) and bilateral guided upsampling (BGU) (Chen et al., 2016) by approximation accuracy and computational time. Also, we compared the proposed method with naïve implementation, which does not subsample images, in computational time. For the proposed method, we also compared the fast local LUT upsampling (FastLLU) with the conventional approach of local LUT upsampling (LLU), which use WTA for local LUT generation. Also, we evaluated tri-linear interpolation and linear-bicubic interpolation for interpolating the local LUT. We utilized eight high-resolution test images: artificial ( $3072 \times 2048$ ), bridge ( $2749 \times 4049$ ), building ( $7216 \times 5412$ ), cathedral ( $2000 \times 3008$ ), deer ( $4043 \times 2641$ ), fireworks ( $3136 \times 2352$ ), flower ( $2268 \times 1512$ ), tree ( $6088 \times 4550$ ). We used peak-signal noise ratio (PSNR) for accuracy evaluation, and we regarded the results of the naïve filtering as ground truth results.

We implemented the proposed method by C++ with OpenMP parallelization. We also used Intel IPP for the cubic upsampling, which is optimized by AVX/AVX2. For guided image upsampling, we also optimized by AVX/AVX2 with OpenCV functions. For downsampling in the proposed method, we use the nearest neighbor downsampling. For this downsampling, we used OpenCV and Intel IPP for the operation with `cv::INTER_NN` option. The used computer was Intel Core i7 6700 (3.40 GHz) and compiled by Visual Studio 2017. We used  $r = 2$  for local LUT upsampling,  $iteration = 10$ ,  $\sigma_s = 10$ ,  $\sigma_c = 20$ ,  $r = 3\sigma_s$  for iterative bilateral filtering, and  $\lambda = 0.01$  and  $\kappa = 1.5$  for  $L_0$  smoothing. PSNR and computational time are averages of eight high-resolution images.

Figure 4 shows the PSNR accuracy of each acceleration method for iterative bilateral filtering and  $L_0$  smoothing, respectively. The number of bins of the proposed method is 128. The local LUT based methods, which are LLU and the proposed method of fastLLU, have higher PSNR than other acceleration methods. Note that a subsampling rate of  $1/16$  indicates that the height and the width of images are multiplied by  $1/4$ . Table 1 shows detail information for LLU and fastLLU. The proposed method of fastLLU



(a) Iterative bilateral filtering



(b)  $L_0$  smoothing

Figure 4: Approximation accuracy of PSNR for each acceleration method with changing subsampling rate.

is slightly better than the conventional approach of LLU.

Figure 5 shows the computational time of each acceleration method for two edge-preserving filters. The horizontal line of the graph shows the computational time of naïve implementation. The computational time is an average of 10 trials. The fastLLU is the second fastest of five methods, which is  $\times 100$  faster than the naïve implementation when the subsampling rate is  $1/64$ . Cubic upsampling is simple and fast, but the performance is not high.

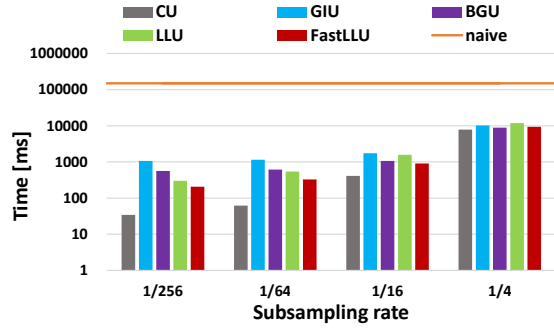
Figure 6 shows the trade-off between the PSNR accuracy and the computational time by changing the subsampling rate from  $1/4$  to  $1/256$ . Results show that the fastLLU has the best performance in this trade-off among these acceleration methods.

Figure 7 also shows the trade-off between the PSNR accuracy and the computational time of local LUT based methods. The result shows that the FLL based upsampling (fastLLU) is faster than the WTA based local LUT upsampling (LLU), and also have a little higher PSNR. The result also shows that using bicubic interpolation for spatial domain obtains slight higher PSNR, though it takes a longer time.

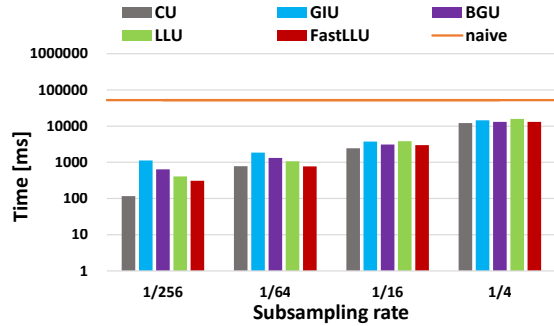
Figure 8 show the relationship between spatial/intensity subsampling rate and PSNR for iterative

Table 1: Approximation accuracy of PSNR for LLU and FastLLU (FLLU).

	Iterative bilateral filtering		$L_0$ smoothing	
	LLU	FLLU	LLU	FLLU
1/1024	26.296	26.322	31.652	31.675
1/256	28.377	28.460	32.548	32.572
1/64	31.985	32.023	33.774	33.798
1/16	34.438	34.465	35.568	35.598
1/4	37.340	37.367	38.373	38.422



(a) Iterative bilateral filtering



(b)  $L_0$  smoothing

Figure 5: Computational time for naïve implementation and each acceleration method with changing subsampling rate.

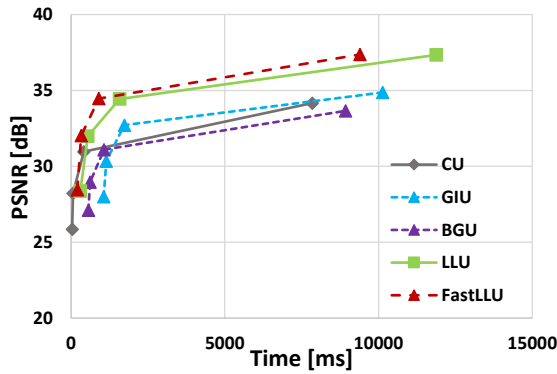
bilateral filtering. The spatial subsampling has a more significant effect than the range subsampling.

Figures 9 and 10 depict input image and results of each acceleration method for iterative bilateral filtering and  $L_0$  smoothing, respectively. We omit the result of LLU because the result is similar to the FastLLU.

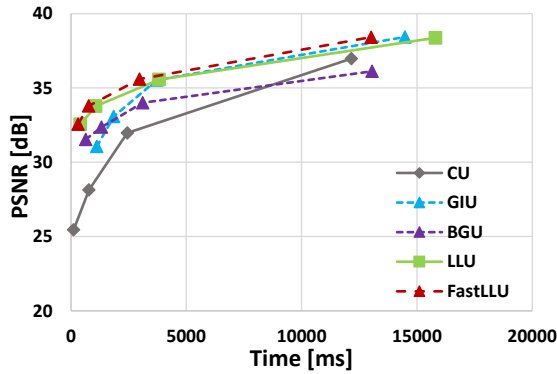
Figure 11 depict results of each approach of the proposed method for  $L_0$  smoothing.

## 5 CONCLUSIONS

In this paper, we proposed an acceleration method for edge-preserving filtering with image upsampling. The local LUT upsampling has higher approximation accuracy than conventional methods. Also, the lo-



(a) Iterative bilateral filtering



(b)  $L_0$  smoothing

Figure 6: Changing subsampling rate performance in PSNR w.r.t. the computational time of each acceleration method.

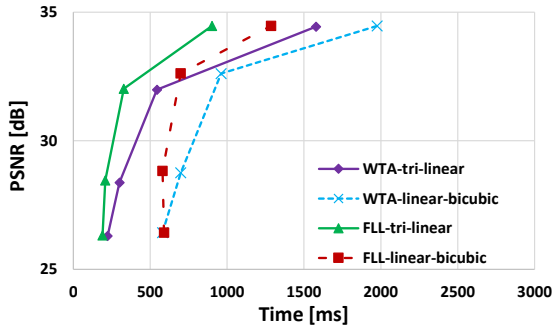


Figure 7: Changing subsampling rate performance in PSNR w.r.t. the computational time of each approach for the proposed (Iterative bilateral filtering).

cal LUT upsampling accelerates  $\times 100$  faster than the naïve implementation. We also described that fast LUT upsampling could obtain a higher approximation of accuracy and faster computational time than using the WTA approach. Also, by using bicubic interpolation, the proposed method can output more accurate results.

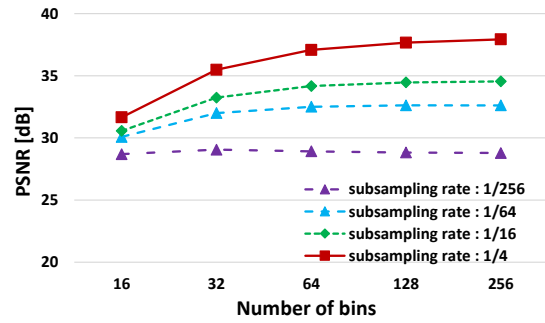


Figure 8: Accuracy of PSNR by changing the number of bins for the proposed method (Iterative bilateral filtering).

## ACKNOWLEDGEMENTS

This work was supported by JSPS KAKENHI (JP17H01764, 18K18076, 19K24368).

## REFERENCES

- Adams, A., Baek, J., and Davis, M. A. (2010). Fast high-dimensional filtering using the permutohedral lattice. *Computer Graphics Forum*, 29(2):753–762.
- Aubry, M., Paris, S., Hasinoff, S. W., Kautz, J., and Durand, F. (2014). Fast local laplacian filters: Theory and applications. *ACM Transactions on Graphics*, 33(5).
- Bae, S., Paris, S., and Durand, F. (2006). Two-scale tone management for photographic look. *ACM Transactions on Graphics*, pages 637–645.
- Buades, A., Coll, B., and Morel, J. M. (2005). A non-local algorithm for image denoising. In *Proc. Computer Vision and Pattern Recognition (CVPR)*.
- Chaudhury, K. N. (2011). Constant-time filtering using shiftable kernels. *IEEE Signal Processing Letters*, 18(11):651–654.
- Chaudhury, K. N. (2013). Acceleration of the shiftable  $o(1)$  algorithm for bilateral filtering and nonlocal means. *IEEE Transactions on Image Processing*, 22(4):1291–1300.
- Chaudhury, K. N., Sage, D., and Unser, M. (2011). Fast  $o(1)$  bilateral filtering using trigonometric range kernels. *IEEE Transactions on Image Processing*, 20(12):3376–3382.
- Chen, J., Adams, A., Wadhwa, N., and Hasinoff, S. W. (2016). Bilateral guided upsampling. *ACM Trans. Graph.*, 35(6):203:1–203:8.
- Dabov, K., Foi, A., Katkovnik, V., and Egiazarian, K. (2007). Image denoising by sparse 3-d transform-domain collaborative filtering. *IEEE Transactions on image processing*, 16(8):2080–2095.
- Durand, F. and Dorsey, J. (2002). Fast bilateral filtering for the display of high-dynamic-range images. *ACM Transactions on Graphics*, 21(3):257–266.

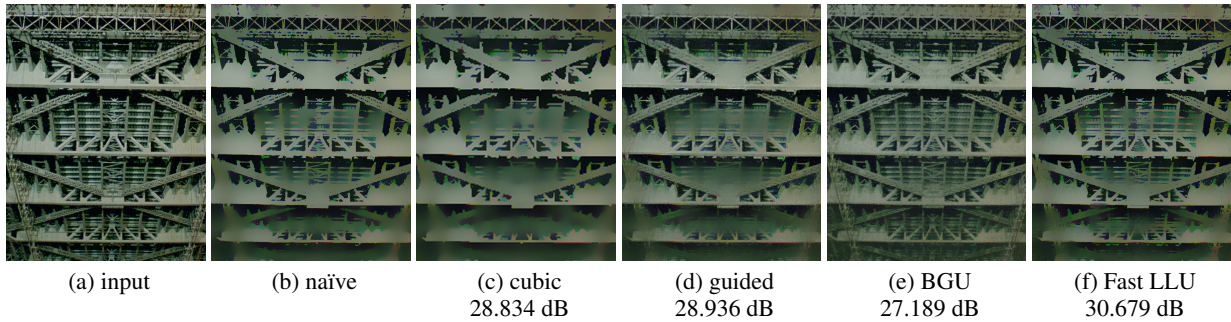


Figure 9: Results of iterative bilateral filtering.

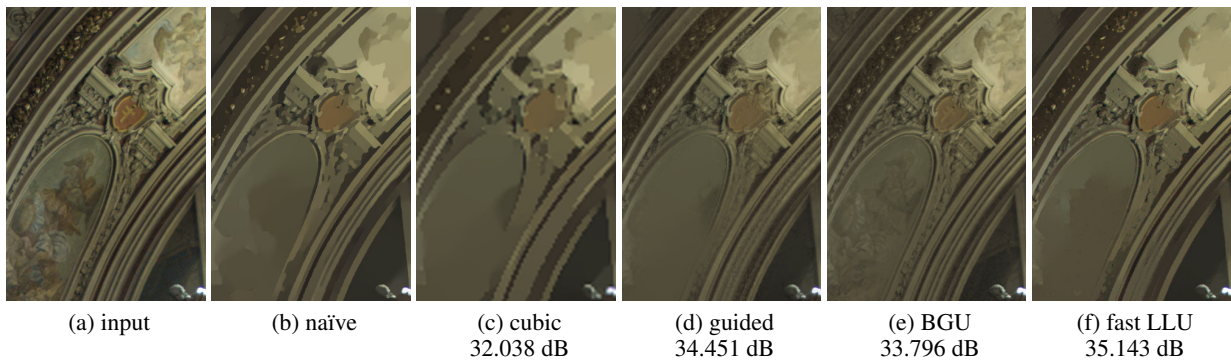


Figure 10: Results of  $L_0$  smoothing.

- Eisemann, E. and Durand, F. (2004). Flash photography enhancement via intrinsic relighting. *ACM Transactions on Graphics*, 23(3):673–678.
- Fujita, S., Fukushima, N., Kimura, M., and Ishibashi, Y. (2015). Randomized redundant dct: Efficient denoising by using random subsampling of dct patches. In *Proc. ACM SIGGRAPH Asia 2015 Technical Briefs*.
- Fukushima, N., Fujita, S., and Ishibashi, Y. (2015). Switching dual kernels for separable edge-preserving filtering. In *Proc. IEEE International Conference on Acoustics, Speech and Signal Processing (ICASSP)*.
- Fukushima, N., Kawasaki, Y., and Maeda, Y. (2019a). Accelerating redundant dct filtering for deblurring and denoising. In *IEEE International Conference on Image Processing (ICIP)*.
- Fukushima, N., Sugimoto, K., and Kamata, S. (2018). Guided image filtering with arbitrary window function. In *Proc. IEEE International Conference on Acoustics, Speech and Signal Processing (ICASSP)*.
- Fukushima, N., Takeuchi, K., and Kojima, A. (2016). Self-similarity matching with predictive linear upsampling for depth map. In *Proc. 3DTV-Conference*.
- Fukushima, N., Tsubokawa, T., and Maeda, Y. (2019b). Vector addressing for non-sequential sampling in fir image filtering. In *IEEE International Conference on Image Processing (ICIP)*.
- Gastal, E. S. L. and Oliveira, M. M. (2011). Domain transform for edge-aware image and video processing. *ACM Transactions on Graphics*, 30(4).
- Gastal, E. S. L. and Oliveira, M. M. (2012). Adaptive manifolds for real-time high-dimensional filtering. *ACM Transactions on Graphics*, 31(4).
- Ghosh, S., Nair, P., and Chaudhury, K. N. (2018). Optimized fourier bilateral filtering. *IEEE Signal Processing Letters*, 25(10):1555–1559.
- He, K. and Sun, J. (2015). Fast guided filter. *CoRR*, abs/1505.00996.
- He, K., Sun, J., and Tang, X. (2009). Single image haze removal using dark channel prior. In *Proc. Computer Vision and Pattern Recognition (CVPR)*.
- He, K., Sun, J., and Tang, X. (2010). Guided image filtering. In *Proc. European Conference on Computer Vision (ECCV)*.
- Hennessy, J. L. and Patterson, D. A. (2017). *Computer Architecture, Sixth Edition: A Quantitative Approach*. Morgan Kaufmann Publishers Inc., San Francisco, CA, USA, 6th edition.
- Hosni, A., Rhemann, C., Bleyer, M., Rother, C., and Gelautz, M. (2013). Fast cost-volume filtering for visual correspondence and beyond. *IEEE Transactions on Pattern Analysis and Machine Intelligence*, 35(2):504–511.
- Kodera, N., Fukushima, N., and Ishibashi, Y. (2013). Filter based alpha matting for depth image based rendering. In *Proc. IEEE Visual Communications and Image Processing (VCIP)*.
- Kopf, J., Cohen, M. F., Lischinski, D., and Uyttendaele, M.

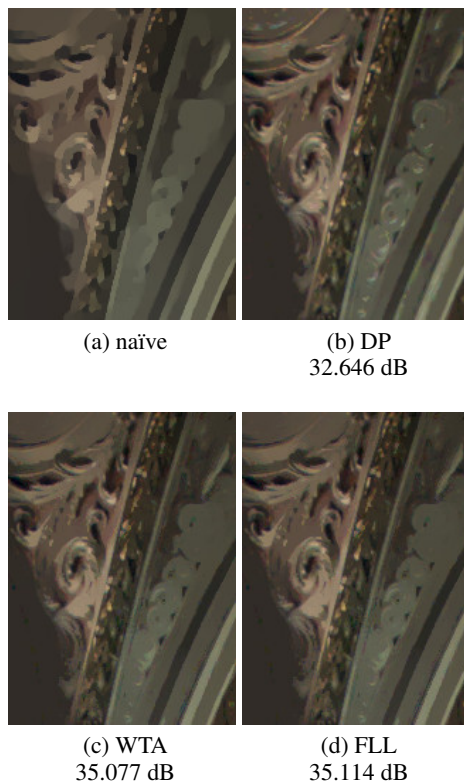


Figure 11: Results of each approach for the proposed.

- (2007). Joint bilateral upsampling. *ACM Transactions on Graphics*, 26(3).
- Levin, A., Lischinski, D., and Weiss, Y. (2004). Colorization using optimization. *ACM Transactions on Graphics*, 23(3):689–694.
- Maeda, Y., Fukushima, N., and Matsuo, H. (2018a). Effective implementation of edge-preserving filtering on cpu microarchitectures. *Applied Sciences*, 8(10).
- Maeda, Y., Fukushima, N., and Matsuo, H. (2018b). Taxonomy of vectorization patterns of programming for fir image filters using kernel subsampling and new one. *Applied Sciences*, 8(8).
- Matsuo, T., Fujita, S., Fukushima, N., and Ishibashi, Y. (2015). Efficient edge-awareness propagation via single-map filtering for edge-preserving stereo matching. In *Proc. SPIE*, volume 9393.
- Matsuo, T., Fukushima, N., and Ishibashi, Y. (2013). Weighted joint bilateral filter with slope depth compensation filter for depth map refinement. In *Proc. International Conference on Computer Vision Theory and Applications (VISAPP)*.
- Min, D., Choi, S., Lu, J., Ham, B., Sohn, K., and Do, M. N. (2014). Fast global image smoothing based on weighted least squares. *IEEE Transactions on Image Processing*, 23(12):5638–5653.
- Murooka, Y., Maeda, Y., Nakamura, M., Sasaki, T., and Fukushima, N. (2018). Principal component analysis for acceleration of color guided image filtering. In

*Proc. International Workshop on Frontiers of Computer Vision (IW-FCV)*.

- Paris, S., Hasinoff, S. W., and Kautz, J. (2011). Local laplacian filters: Edge-aware image processing with a laplacian pyramid. pages 68:1–68:12.
- Petschnigg, G., Agrawala, M., Hoppe, H., Szeliski, R., Cohen, M., and Toyama, K. (2004). Digital photography with flash and no-flash image pairs. *ACM Transactions on Graphics*, 23(3):664–672.
- Sugimoto, K., Fukushima, N., and Kamata, S. (2016). Fast bilateral filter for multichannel images via soft-assignment coding. In *Proc. Asia-Pacific Signal and Information Processing Association Annual Summit and Conference (APSIPA)*.
- Sugimoto, K., Fukushima, N., and Kamata, S. (2019). 200 fps constant-time bilateral filter using svd and tiling strategy. In *IEEE International Conference on Image Processing (ICIP)*.
- Sugimoto, K. and Kamata, S. (2015). Compressive bilateral filtering. *IEEE Transactions on Image Processing*, 24(11):3357–3369.
- Tajima, H., Fukushima, N., Maeda, Y., and Tsubokawa, T. (2019). Local lut upsampling for acceleration of edge-preserving filtering.
- Tomasi, C. and Manduchi, R. (1998). Bilateral filtering for gray and color images. In *Proc. International Conference on Computer Vision (ICCV)*, pages 839–846.
- Xu, L., Lu, C., Xu, Y., and Jia, J. (2011). Image smoothing via l0 gradient minimization. *ACM Transactions on Graphics*.
- Yang, Q., Tan, K. H., and Ahuja, N. (2009). Real-time o(1) bilateral filtering. In *Proc. Computer Vision and Pattern Recognition (CVPR)*, pages 557–564.
- Yu, G. and Sapiro, G. (2011). Dct image denoising: A simple and effective image denoising algorithm. *Image Processing On Line*, 1:1.